

## Research Papers

# Effect of electrode surface treatment on carbon fiber based structural supercapacitors: Electrochemical analysis, mechanical performance and proof-of-concept

Joaquín Artigas-Arnaudas<sup>\*</sup>, Xoan F. Sánchez-Romate, María Sánchez, Alejandro Ureña

Materials Science and Engineering Area, Escuela Superior de Ciencias Experimentales y Tecnología, Universidad Rey Juan Carlos, Calle Tulipán s/n, 28933 Móstoles, Madrid, Spain



## ARTICLE INFO

## Keywords:

Structural supercapacitor  
Multifunctional composite  
Carbon fiber  
Interlaminar properties  
Electrochemical behavior

## ABSTRACT

Supercapacitors based on carbon fiber reinforced polymer (CFRPs) were studied and the influence of surface treatment on mechanical and electrochemical properties was explored. Electrodes were prepared by deposition of graphene nanoplatelets (GNPs) combined with different binders (PVDF and PVA) onto the surface of a carbon fiber fabric. A significant decrease in the Interlaminar Shear Strength (ILSS) is observed when comparing the solid polymer electrolyte to the structural resin (around 50 %). Moreover, the addition of any binder promotes a decrease in the ILSS due to lower interfacial properties (around 20 % when compared to the GNP-coated condition). Electrochemical impedance spectroscopy (EIS) analysis proves that the structural capacitor can be fitted with an equivalent circuit consisting of R-CPE series elements. An increase of the bulk resistance was observed when using a binder (29.7 and 22.7 k $\Omega$ ) when compared to the GNP-only-coated (10.2 k $\Omega$ ). For this reason, the structural supercapacitor with the best properties was the GNP-only-coated one with a specific capacitance and coulombic efficiency, calculated by Galvanostatic charge-discharge (GCD), of 5.2 mF/g, showing also high stability of electrochemical properties over time. Energy storage capability was successfully demonstrated by a proof of concept consisting of powering a LED after a short charge time of the device.

## 1. Introduction

Sustainable energy consumption and climate change are worldwide concerns. Energy demand and sustainability are a world-rising concerns. Several efforts and actions have been taken to reduce the emission of greenhouse gases such as CO<sub>2</sub> or N<sub>2</sub>O. In this regard, there is an ongoing interest in the use of alternative clean energy to power road transportation as it is one of the main important sources of this kind of pollution [1,2]. The electric vehicle (EV) development has exploded in the last few years as an alternative to reduce the consumption of fossil fuel and gas emissions [3,4]. Electric energy can be produced from cleaner and renewable sources and then be stored. The autonomy of an electric vehicle depends on battery capacity [5]. To compete with conventional and hybrid vehicles there is a need to increase the time between charges. This has driven the industry and researchers to improve energy storage devices for electric mobility [6].

Overall weight reduction can lead to more efficient use of energy to power electric engines and to improve EV autonomy [7]. Here, carbon

fiber reinforced polymers (CFRPs) have been extensively used for structural components in transport applications such as automotive and aerospace. The traditional lightweight alloys are being replaced by CFRP thanks to their combination of exceptional mechanical and physical properties. More specifically, composite materials are already used at an important percentage of aircraft components, especially structural ones [8,9]. This could lead to a reduction of costs and expand its use in the automotive industry. Also, there is an increasing effort to broaden the range of CFRP applications by developing multifunctional materials. For EV, the development of structural energy storage devices is an interesting alternative. These components could cover the mechanical requirements of structural elements and store the electric energy needed to power the vehicle [10–12]. This way, the weight of the main batteries can be reduced by using for this purpose an already existing structural component.

Electrochemical Double Layer Capacitors (EDLCs) or supercapacitors are devices that present higher energy density than electrolytic capacitors and more specific power than rechargeable batteries [13]. They

<sup>\*</sup> Corresponding author.

E-mail address: [joaquin.artigas@urjc.es](mailto:joaquin.artigas@urjc.es) (J. Artigas-Arnaudas).

<https://doi.org/10.1016/j.est.2022.106599>

Received 30 October 2022; Received in revised form 15 December 2022; Accepted 30 December 2022

Available online 5 January 2023

2352-152X/© 2023 The Authors. Published by Elsevier Ltd. This is an open access article under the CC BY license (<http://creativecommons.org/licenses/by/4.0/>).

consist of two electrodes and a dielectric layer as a separator in between, all embedded in an electrolyte. A crucial factor for their energy storage properties is the high surface area of the electrodes [14,15], as well as the ionic conductivity of the electrolyte. In this context, electrodes are usually made of porous carbon materials, metal oxides, and combinations of them [16,17]. Porous carbon materials can be generated by synthesis [18,19] and carbonization of different template materials [20–22]. Structural supercapacitors based on CFRP can be built using carbon fiber layers as electrodes to make use of its mechanical properties and electric conductivity, glass fiber can be used as a separator, and polymeric resin as a solid electrolyte [23]. The elements of a structural supercapacitor are schematically represented in Fig. 1.

In order to improve the capacitance of carbon fiber electrodes, different strategies have been followed to increase the surface area of the fiber. The activation of carbon fiber was one of the first alternatives [24,25]. Also, it has been studied the direct synthesis of porous carbon structures and nanoparticles such as carbon aerogels [26,27] or carbon nanotubes (CNTs) [28,29], and metal oxides like CuO, ZnO, or NiO [30–32]. Although there is an improvement in capacitance, there is also a negative effect on mechanical properties as the surface of the fiber is directly altered [33]. Therefore, it has been shown that the deposition of carbon nanoparticles, such as graphene nanoplatelets (GNPs), may increase capacitance without a severe detriment to mechanical properties [34,35]. To ensure the adhesion of the particles in the electrode, different binders have been used [36]. These binders keep the structure of the electrode and create a framework of connected particles. Poly(vinylidene difluoride) (PVDF) and polyvinyl alcohol (PVA) are common polymers used as an electrolyte for flexible energy storage devices where both electrochemical and mechanical properties are needed [37,38]. Therefore, PVDF and PVA have been chosen as possible binders for carbon fiber electrodes. These binders have been used in structural supercapacitors demonstrating energy storage capacity and mechanical performance [39,40].

Solid-state electrolytes are used as matrices in structural supercapacitors. They need to present a good combination of ionic conductivity to allow charge mobility and mechanical properties good enough to fulfill the structural requirements [41]. This is usually achieved by the mixture of structural polymeric resins with ion-conductive elements such as ionic liquids [42]. Different studies have found that the increasing crosslinking degree of structural resin promotes a decrease in ionic transport [43,44]. In this regard, recent studies have found a good balance of properties by adding Al<sub>2</sub>O<sub>3</sub> nanoparticles into the solid-state electrolyte [45].

The multifunctional behavior of structural supercapacitors has been characterized by analyzing both mechanical and electrochemical performances. For mechanical properties, tensile tests are usually performed on these composites [26,30,31,46]. However, the behavior of the interface matrix-fiber is critical in composite materials to ensure the distribution of mechanical stresses. Therefore, Interlaminar Shear Strength tests (ILSS) are also commonly used to evaluate the shear properties of the matrix and the interface. Nevertheless, this kind of test has not been reported for structural supercapacitors.

This study is focused, thus, on both mechanical and electrochemical

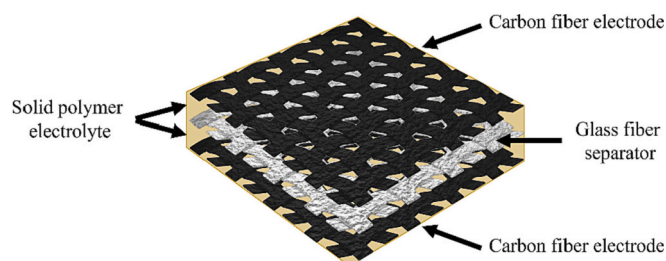


Fig. 1. Schematics of a CFRP structural supercapacitor.

analysis of structural supercapacitors made of carbon fiber electrodes and solid polymer electrolytes. Electrodes have been prepared by spray coating, an industrial-accessible processing route to deposit the GNPs on the surface of the carbon fiber fabrics. Different electrodes have been prepared using different binders to evaluate their influence on the final device properties. All the cells have been manufactured by Vacuum Assisted Resin Infusion Moulding (VARIM) as it ensures good final properties and cost-efficiency. Images of structural supercapacitor cross-sections were analyzed and correlated with mechanical results from ILSS tests. Moreover, electrochemical properties were also evaluated by calculation of specific capacitance and analysis of Electrochemical Impedance Spectroscopy (EIS). Finally, as a proof of concept, a LED has been powered with the structural supercapacitor to show the energy storage capability. Here, it is important to point out that the development of structural capacitors will be very important, not only for the automotive industry but also for other applications such as unmanned aerial vehicles, wind turbine blades, or buildings [47], where the necessity of structural storage materials are very high.

## 2. Experimental

### 2.1. Materials

Electrodes were made from a woven carbon fiber (CF) *HexForce*<sup>TM</sup> *AGP280-5H*. It is a bi-axial 0/90 AS4 GP 3 K satin weave fabric supplied by *Hexcel*. Glass fiber (GF) *E-Fiberglass* woven roving supplied by *Castro Composites*<sup>TM</sup> was used as a separator. The electrode CF layer presents a specific weight of 285 g/m<sup>2</sup> while the GF separator is 110 g/m<sup>2</sup>.

Graphene nanoplatelets (GNPs) were *xGNP 750 Grade C* supplied by *XGScience*. They were chosen because of their average size, 2 μm diameter and 2 nm thickness, and high specific surface area, 750 g/m<sup>2</sup>. Poly(vinylidene fluoride) (PVDF) binder *Kynar HSV 900* was supplied by *Arkema*. Poly (vinyl alcohol) (PVA) binder with molecular weight between 30,000 and 70,000 was provided by *SigmaAldrich*. Additionally, the surfactant *Triton X-100* was used to improve the dispersion of GNPs and N,N-dimethylformamide (DMF) as the solvent, both supplied by *SigmaAldrich*.

Solid polymer electrolyte is composed of two resin systems. The structural resin was an epoxy-based *Araldite LY556* with an amino-hardener *XB3473*, supplied by *Huntsman*, in a weight proportion of 100:23 (monomer to hardener). The second system was a Poly(ethylene glycol) diglycidyl ether (PEGDGE) based resin with a 4-Aminophenyl sulfone (DDS) hardener, in a 100:35 proportion. Ionic liquid (IL) *EMITSFI*, supplied by *IoLiTec*, was also included to improve ionic mobility. Finally, to improve the electrochemical performances Al<sub>2</sub>O<sub>3</sub> nanoparticles were added. They were supplied by *SigmaAldrich* with an average size of 13 nm.

### 2.2. Manufacturing of CFRP electrodes

Two different types of electrodes were prepared depending on the binder used to fix the GNPs to the surface of the woven carbon fiber. For each binder, a different solvent dispersion of 3 wt% GNPs was prepared. The first dispersion consisted of 1 wt% PVDF and GNPs in DMF. Alternatively, 1 wt% PVA, 0.3 wt% *Triton x-100*, and GNPs were mixed in water. Finally, the dispersion of GNPs in both solvent solutions was generated by ultrasonication for 30 min.

Electrodes were prepared by spray coating. Dispersions of GNPs were sprayed onto the surface of woven carbon fiber with a manual spray gun *Krippe 840-LP* at 1 bar and 20 cm distance. Before any deposition, carbon fabrics were washed with acetone and dried in an oven. The deposition was performed on both sides of the fabric, leaving the coating to dry at 100 °C for 10 min between each side deposition. Finally, the remaining solvent was evaporated by heating the carbon fibers in an oven for 1 h at 100 °C.

### 2.3. Manufacturing of CFRP structural supercapacitors

Different cells were manufactured to test each kind of electrode. Structural supercapacitors were built with a symmetric cell structure, each electrode was composed of one layer of modified woven carbon fiber and they were separated by two layers of glass fiber. The final architecture of the supercapacitor cell was CF/GF/GF/CF. For the mechanical analysis, composites were built in alternating layers of CF and GF until reaching the desired thickness.

Solid polymer electrolyte prepared as the matrix for the composite was composed of a 44.2 wt% of LY556/XB3473 resin system, 23.8 wt% of PEGDGE/DDS system, 30 wt% EMITSFI and 2 wt% of Al<sub>2</sub>O<sub>3</sub> nanoparticles. These proportions were optimized in previous studies [45]. First, LY556, PEGDGE, and EMITSFI were mixed by magnetic stirring at 80 °C for 30 min under vacuum conditions to remove the possible entrapped air. Al<sub>2</sub>O<sub>3</sub> nanoparticles were added to the mixture and dispersed by ultrasonication for 45 min. Hardeners XB3473 and DDS were added after the dispersion and the mixture was degasified again at 80 °C for 10 min before the infusion.

For comparison, the same composites were manufactured with only the structural base resin components in a proportion of 65 wt% LY556/XB3473 and 35 wt% PEGDGE/DDS. Here, the aim was to explore their mechanical properties in comparison to the developed solid polymer electrolyte-based composites.

Composite manufacture was carried out by vacuum-assisted resin infusion moulding (VARIM) technique with a similar set-up used previously [48] as shown in Fig. 2.

### 2.4. Microstructural characterization

Evaluation of the coatings was performed using a Scanning Electron Microscope (SEM), S-3400 N by Hitachi. SEM images were also used to study the cross-section of the composites and the evaluation of the failure mode during mechanical characterization. In this case, the samples were coated with a thin layer of gold by sputtering for proper characterization.

### 2.5. Electrochemical analysis

Electrochemical tests were conducted with a PGSTAT302N potentiostat from Autolab. To ensure electrical contact, a copper sheet was attached to the surface of each CF electrode after manufacturing. Cyclic voltammetry (CV) tests were carried out at a scan rate of 5 mV/s in a voltage window of -1 to 1 V for a qualitative study. Galvanostatic charge-discharge (GCD) tests were used to study the evolution of specific gravimetric capacitance and coulombic efficiency. A constant current density of 0.02 mA/g was applied for charge until reaching a maximum voltage of 1 V. Same current density was applied during discharge.

Additionally, Electrochemical Impedance Spectroscopy (EIS) was performed by applying a voltage of 30 mV in a frequency range of 0.01 to 10<sup>6</sup> Hz. All electrochemical tests were performed at room

temperature. EIS curves were then fitted to an equivalent circuit with the software Nova 2.1 to describe the response of the elements that compose it.

### 2.6. Mechanical analysis

Interlaminar shear strength (ILSS) tests were used to characterize the mechanical properties. Tests were conducted accordingly to ASTM D2344 at a crosshead speed of 1 mm/min in a universal tensile machine Zwick with a 100 kN load cell. Five specimens of 24 × 8 × 3.5 mm<sup>3</sup> were tested for each condition.

## 3. Results and discussion

In this section, microstructural analysis of carbon fiber (CF) electrodes is carried out by investigating the effect of surface treatment on the morphology of the electrodes. Then, the mechanical and electrochemical properties are evaluated under ILSS and EIS and CV, respectively, to further explore the effect of modified carbon fibers as electrodes on them. Finally, a proof-of-concept by powering a LED is conducted, to prove the functionality of the developed structural supercapacitor.

### 3.1. Microstructural analysis of CF electrodes

The surfaces of modified carbon fibers were initially characterized by SEM analysis, as shown in Fig. 3. In every case, many GNP agglomerates can be observed, regardless of the surface treatment. This behavior is common when depositing carbon nanoparticles due to their high surface energy which promotes the creation of the mentioned aggregates. However, although the presence of aggregates is observed in every case, there is a higher trend to form larger agglomerates with PVA and PVDF. GNP-coated fiber without binder shows a surface fully covered by the nanoparticles with some small agglomerates (Fig. 3a). In this regard, the use of a binder can improve the adhesion of the nanoparticles to the surface, a key parameter that must be taken into account during the processing of the CFRPs, but also between the nanoparticles themselves. The presence of the aggregates is more prevalent in the case of PVA and PVDF-treated carbon fibers (Fig. 3b and c, respectively). The presence of these large agglomerates may have a detrimental effect on both mechanical and electrochemical properties. On the one hand, areas, where many nanoparticles are present, will difficult the impregnation of the matrix during composite manufacturing, promoting the presence of regions of low impregnation. On the other hand, from the electrochemical point of view, the presence of large aggregates will reduce the exposed area of the individual nanoparticles, and, therefore, this will be manifested in a reduction of the capacitance of the final supercapacitor. In this regard, from SEM images of Fig. 3b and c, it can be observed that many areas of the carbon fibers are not covered by the nanoparticles, as they are mainly concentrated around the large aggregates created.

### 3.2. Mechanical analysis of CFRP supercapacitors

Fig. 4 shows the ILSS values for the different tested conditions. First, it is important to point out that, in the case of CFRPs with the structural resin (without IL), there are no significant variations among the different conditions. More specifically, it can be observed that there is, even, an increase in the ILSS value for the GNP-coated condition, in absence of any binder. This can be explained accordingly to the toughening mechanisms induced by the GNPs themselves, which may induce a crack bridging effect, delaying the crack propagation during the ILSS test.

In fact, by looking at the SEM images of ILSS samples, it can be noticed that, in the case of GNP-coated ones, the crack propagation is more tortuous (yellow area Fig. 5b) than in the case of uncoated samples (Fig. 5a), highlighting the mentioned crack-bridging effect of the GNPs.

On the other hand, the PVA and PVDF coated samples present ILSS

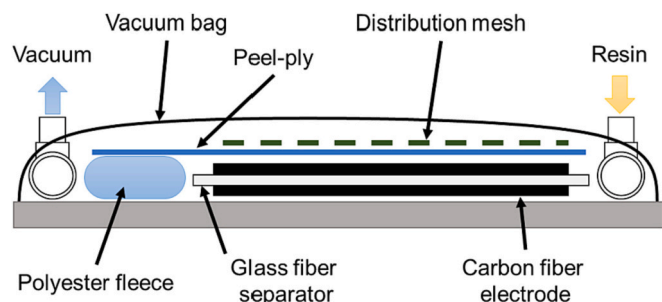
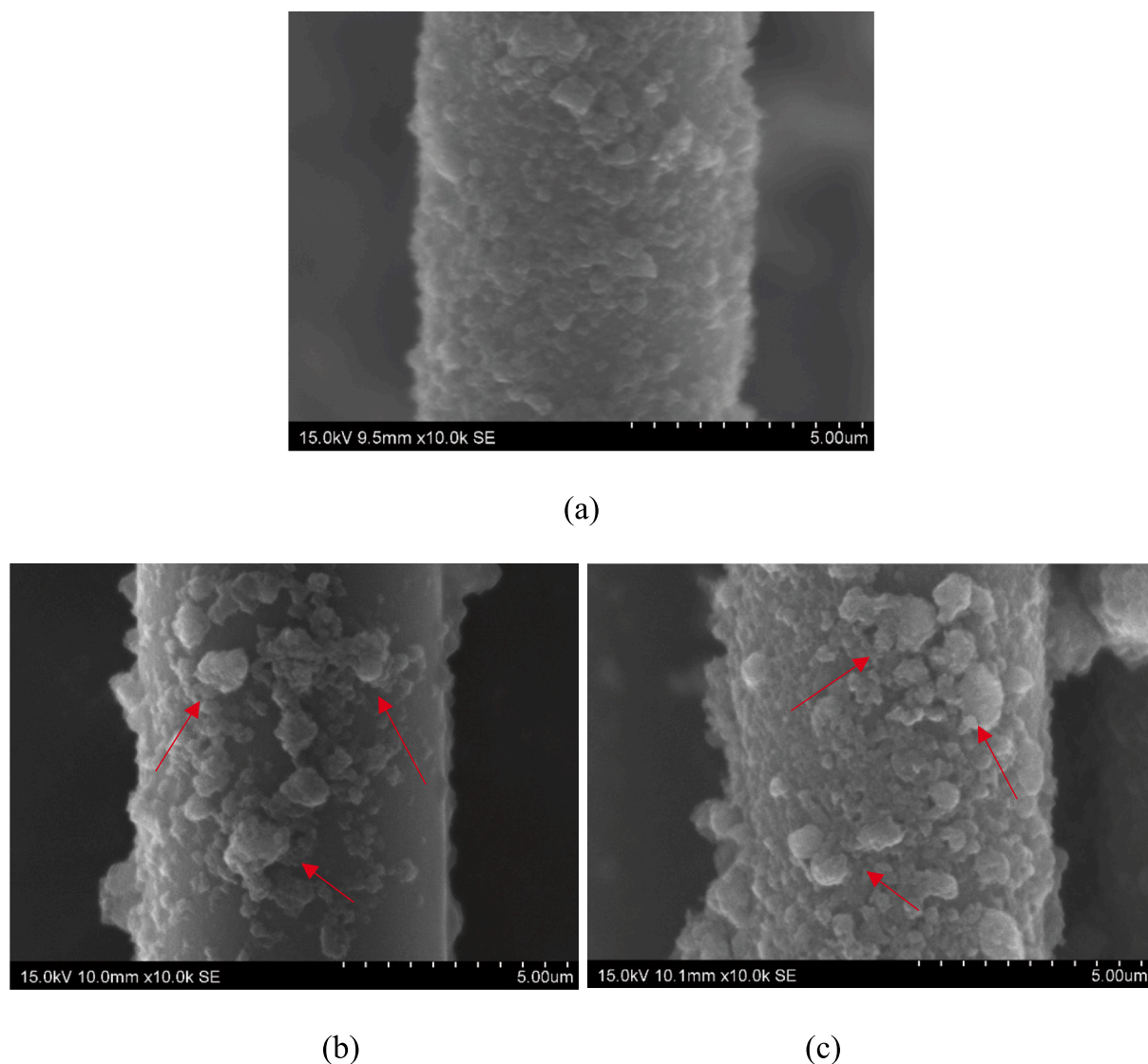


Fig. 2. Schematics of vacuum assisted resin infusion moulding (VARIM) technique.



**Fig. 3.** SEM images of an individual carbon fiber with (a) GNPs (b) PVA-GNPs and (c) PVDF-GNPs surface treatment (the red arrows denote the presence of highly agglomerate GNPs). (For interpretation of the references to colour in this figure legend, the reader is referred to the web version of this article.)

values quite like the uncoated ones, with a slight detriment in the case of PVDF ones. In these cases, the effect of crack bridging given by the GNP coating is reduced by the effect of the binder which may cause a poorer interaction between the carbon fibers and the structural resin. In fact, in these cases, the crack propagation is quite more drastic (Fig. 5c and d), although the differences between the ILSS values are not so significant.

The analysis of the fracture surfaces is in good agreement with the force-displacement curves of the ILSS tests, summarized in Fig. 6, where the GNP-coated sample presents the lower drop of the force during crack propagation, explained by the commented more tortuous crack propagation.

When analyzing the ILSS behavior of the CFRPs with solid polymer electrolytes, however, several important differences can be stated.

On one hand, there is a very significant detriment of the ILSS values among conditions when compared to the structural resin (without IL), with drops of around 50 to 70 % depending on the CFRP surface treatment. These substantial differences are explained by the effect of the matrix. In this case, the mechanical properties of the solid polymer electrolyte are quite below the structural resin, especially in terms of stiffness and strength [42]. Therefore, crack propagation takes place at lower stress values. The detriment of the mechanical properties at the multiscale level has been previously reported in structural

supercapacitors [48]. In addition, the analysis of the force-displacement curves (Fig. 6b) shows that the crack propagation takes place at much lower stress values with, also, a much lower drop of the mechanical response after crack propagation, indicating that it takes place less drastically than in case of structural resin.

On the other hand, it can be noticed that there is an important detriment of the ILSS values when comparing the different CFRP surface treatments. This can be explained accordingly to the interface carbon fiber-matrix evaluated at the cross-section of the composites (Fig. 7).

From SEM images, it can be also observed that the samples with uncoated carbon fibers (Fig. 7a) do not present any resin-poor areas, whereas the samples coated with GNPs and, especially, when using PVA and PVDF binders, present regions with a lack of impregnation (Fig. 7b, c and d). This lack of impregnation is a critical factor, which induces a drastic detriment to the ILSS value. This fact can be apparently contradictory as the viscosity of the solid polymer electrolyte is much lower than the viscosity of the structural resin, however, may be explained accordingly to the manufacturing process. In this case, an over-bleeding can be induced during the VARIM process because of the low viscosity of the solid polymer electrolyte [48], and, therefore, leading to a lack of impregnation in several zones. In addition, the presence of PVA and PVDF binders may alter the compatibility of the carbon fiber with the

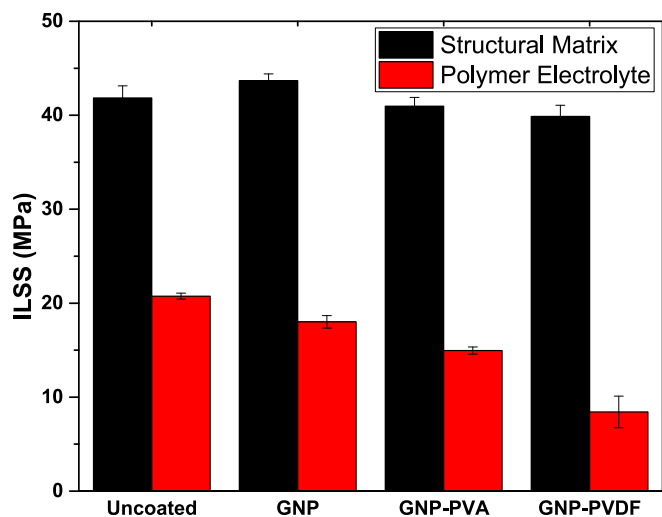
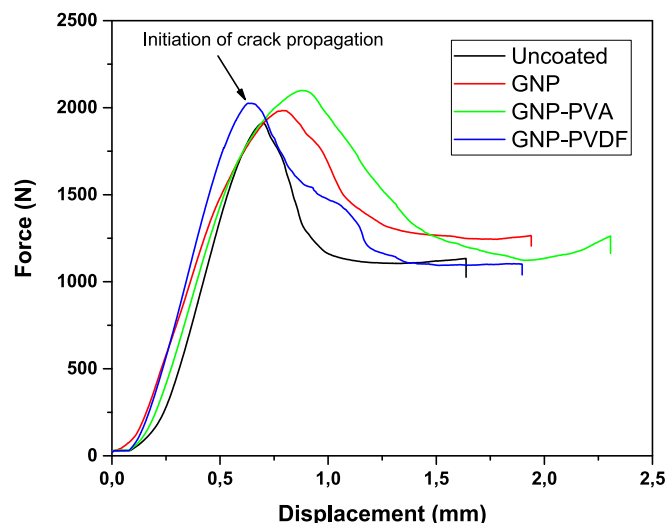
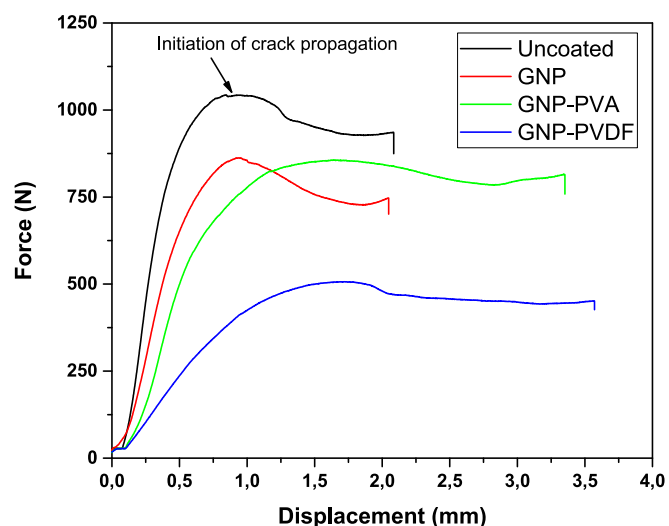
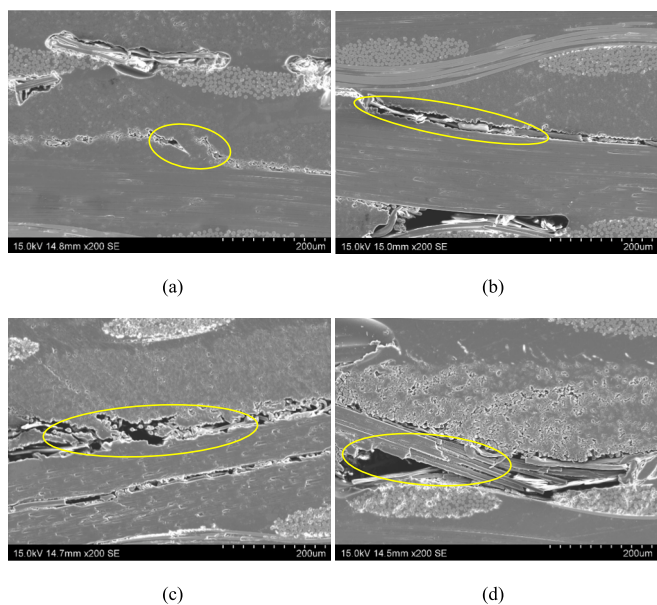


Fig. 4. ILSS values for the different conditions tested where the black columns denote the structural resin and the red ones the solid polymer electrolyte. (For interpretation of the references to colour in this figure legend, the reader is referred to the web version of this article.)



(a)



(b)

Fig. 5. SEM images of CFRPs with structural resin at (a) uncoated, (b) GNP, (c) GNP-PVA and (d) GNP-PVDF conditions. The highlighted regions denote the characteristics of crack propagation in each condition.

solid polymer electrolyte, acting as a lubricant and, thus, inducing a poorer impregnation of the carbon fibers.

Moreover, the crack propagation in these samples takes place, as commented, in a softer way than for the structural resin CFRPs, as the drop of the mechanical force is much lower. This can be also observed in the analysis of the fracture cross sections with the crack propagation pathways, which are quite tortuous (Fig. 7e and red arrows marked in Fig. 7f).

### 3.3. Electrochemical analysis

Cyclic voltammetry curves were used to initially assess and compare the electrochemical behavior of the electrodes. All CV curves shown in Fig. 8 follow the shape pattern of an EDLC cell where no electrochemical peaks are detected as no reactions are produced during the scan. It can

Fig. 6. Force-displacement curves of ILSS test for CFRPs with (a) structural resin and (b) solid polymer electrolyte.

be elucidated that there is a significant difference between the area of the CV curve from the GNPs cell compared to the use of a binder to fix the particles. The specific capacitances ( $C_{sp}$ ) shown in Table 1 are calculated from the area inside the curve by applying the formula of Eq. (1) [49]. Where  $m$  is the mass of the electrodes,  $v$  is the scan rate, and  $V_c - V_a$  is the voltage window, set at 2 V.

$$C_{sp} = \frac{1}{mv(V_c - V_a)} \int_{V_a}^{V_c} IdV \quad (1)$$

In this regard, there is a clear reduction of the capacitance when using the binder (GNP-PVA and GNP-PVDF conditions).

The morphology of the surface of the electrodes, as discussed before, can be correlated with these results. More specifically, nanoparticles

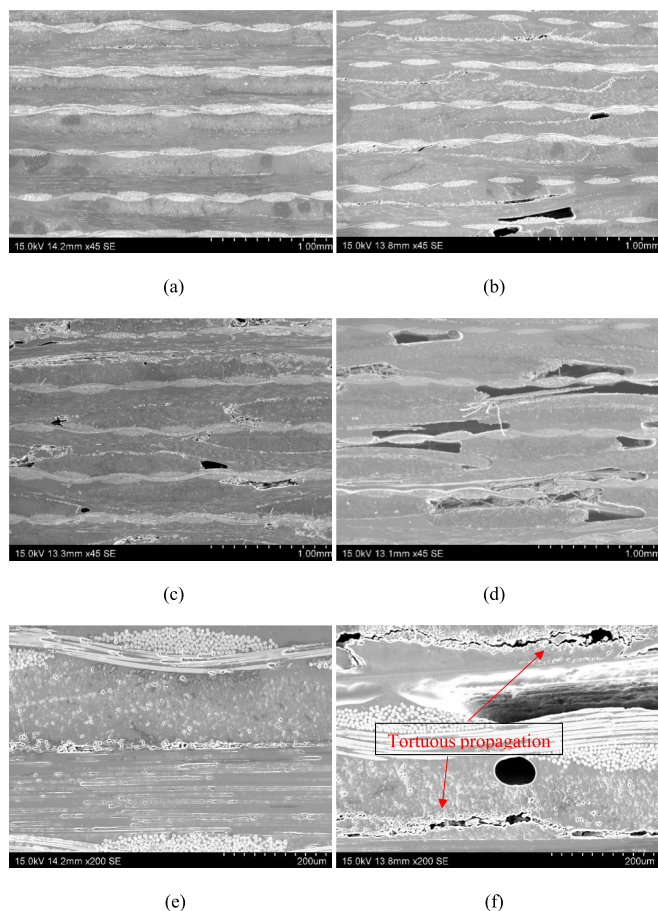


Fig. 7. SEM images of the cross-sections showing the lack of impregnation of (a) uncoated, (b) GNP, (c) GNP-PVA, and (d) GNP-PVDF and showing the crack propagation of (e) uncoated and (f) GNP samples.

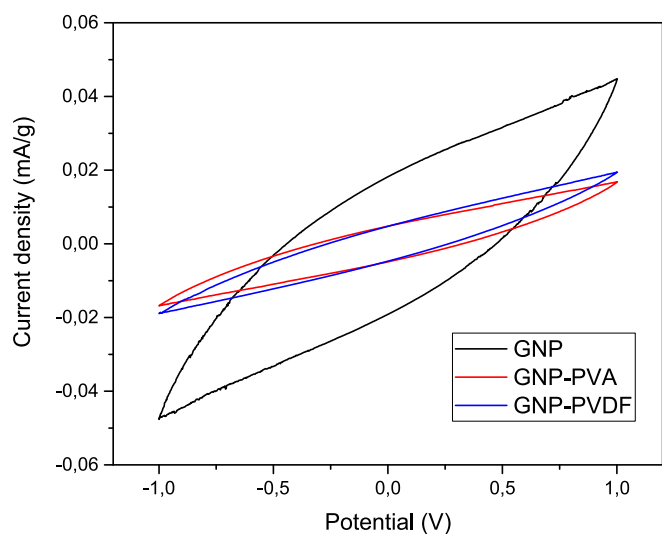


Fig. 8. CV curves of the supercapacitor for the different conditions at a scan rate of 5 mV/s.

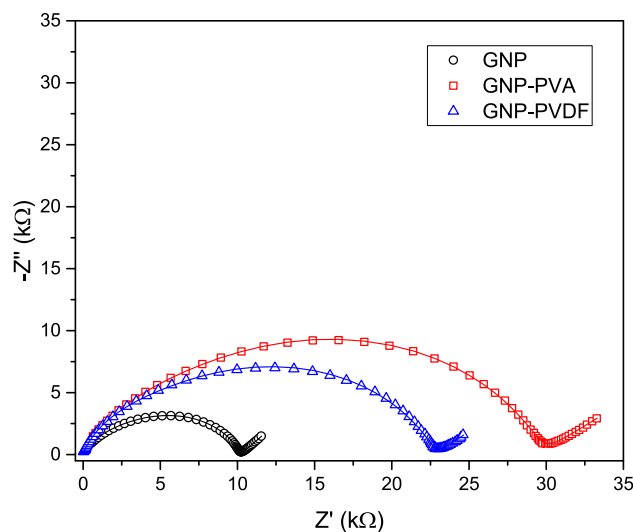
show a high tendency to agglomerate reducing the exposed area for ion mobility. In the case of GNPs electrodes, even with the agglomerates, the solid polymer electrolyte can access more surface area through the porosity between the nanoparticles and the fiber, as the aggregation of nanoparticles is not very prevalent. On the other hand, both binders

Table 1  
Values of capacitance and R/CPE elements for the different tested conditions.

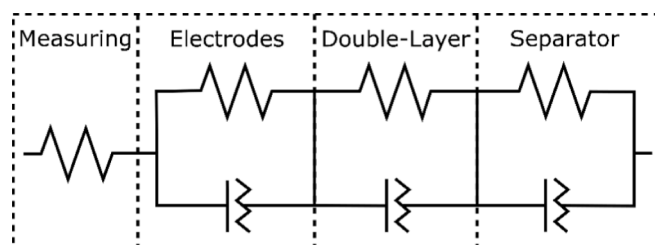
Condition	$C_{SP}$ (mF/g)	Electrode	Double-layer	Separator
		R(k $\Omega$ ) / CPE(n)	R(k $\Omega$ ) / CPE(n)	R(k $\Omega$ ) / CPE(n)
GNP	5.36	3.4 / 0.71	6.8 / 0.71	$1.1 \times 10^9$ / 0.52
GNP-PVA	1.37	6.8 / 0.75	22.9 / 0.78	$1.1 \times 10^9$ / 0.42
GNP-PVDF	1.31	3.8 / 0.85	18.9 / 0.77	$1.1 \times 10^9$ / 0.43

create a layer on top of the fibers, and the agglomerates, which are much more prevalent than in the case of GNPs without binder, block the porosity reducing the surface that the solid polymer electrolyte can cover. Although particles could get fixed to the fiber surface, there is a clear undesirable effect on the electrochemical behavior that promotes a significant reduction of the specific capacitance when adding the binder to the carbon fiber surface.

In order to deepen the analysis of the proposed electrodes, the electrochemical properties of the fabricated supercapacitors were characterized using the EIS technique. Fig. 9a shows the EIS curves obtained for the different treatments applied to the carbon fibers. From the intersection of the curves with the horizontal axis ( $Z'$ ) bulk resistance of the cells can be extracted. Supercapacitors built with GNP-modified electrodes present a resistance of 10.2 k $\Omega$ . A significant increase of bulk resistance was registered for the GNP-PVA and GNP-PVDF, reaching 29.7 and 22.7 k $\Omega$  respectively. This evidence a resistive behavior



(a)



(b)

Fig. 9. (a) EIS curves of the different structural supercapacitors where the solid lines denote the fitted behavior by using (b) the proposed equivalent circuit accordingly to previous studies [48] with Nova 2.1 software (the dots denote the measured data).

associated with the use of binders on the electrodes, which also have a detrimental effect on the capacitance.

It can be observed that the EIS curves are composed of a depressed semicircle at high frequencies followed by an apparent linear behavior at low frequencies. Supercapacitors with carbon electrodes and high conductive electrolyte will present a larger linear behavior at low frequencies [50–52].

This depressed semicircle has been widely observed in other studies [53,54] and denotes the presence of a non-ideal element in the equivalent circuit which can be associated to the bulk properties of the electrolyte and the double-layer at the interface [55,56]. More specifically, the presence of this depressed semicircle is associated with an R-CPE element, where CPE denotes a constant phase element. Here, a CPE is a non-ideal resistive-capacitive element with a constant phase. The R-CPE element could be used to describe the semicircle at high frequencies in relation with the ion migration on polymer electrolytes [56]. The impedance of the CPE,  $Z$ , may be calculated from this expression [57]:

$$Z = \frac{1}{Q_0(j\omega)^n} \quad (2)$$

where  $Q_0$  is a normalization factor related to the capacitance,  $\omega$  the frequency, and  $n$  an exponent that denotes the capacitive behavior of the element. For  $n = 1$ , the CPE is a pure capacitor and for  $n = 0$  a pure resistance.

Furthermore, the first depressed semicircle may be composed of a series of R-CPE elements. In addition, the linear behavior at low frequencies may be actually a depressed semicircle with a very high value of resistance [53], which could also be described by a CPE [55].

Therefore, the final equivalent circuit will be composed of three R-CPE elements (Fig. 9b) as in previous studies [48]. The first one corresponds to the carbon fiber electrodes, the second one will be correlated to the double-layer capacitor and the third one to the glass fiber separator. In this regard, Table 1 summarizes the values of the R-CPE elements. Here, several facts can be stated.

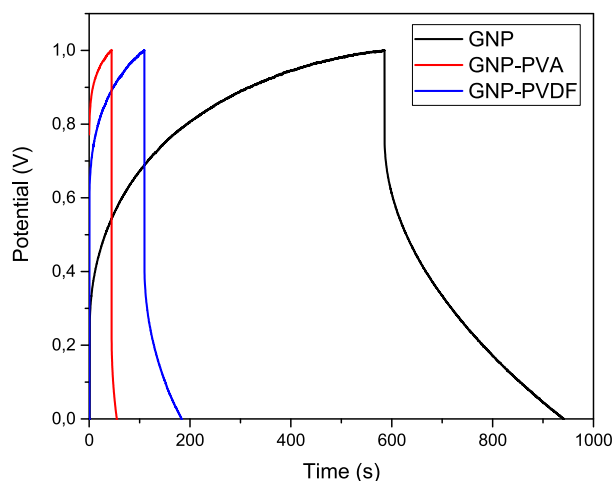
On the one hand, it can be noticed that the GNP-coated supercapacitor in absence of any binder presents the lowest values of the resistance for the first and second semicircles. More specifically, the values of the resistance, which corresponds to the electrodes range from 3.4 to 6.8 k $\Omega$ , indicating that the GNPs are better dispersed into the carbon fiber substrate in absence of any binder.

Furthermore, when comparing the resistance values of the second depressed semicircle (6.8 to 22.9 k $\Omega$ ), the differences are much more prevalent. This can be explained because, as shown in the micrographs of Fig. 7, the samples in absence of PVA or PVDF present the best interfacial properties, without any prevalent lack of impregnation. Therefore, ionic mobility is much more favored. In this regard, the lack of impregnation of the matrix into the fibers due to the presence of the binder prevents effective ionic mobility, which negatively affects the electrochemical properties of these supercapacitors.

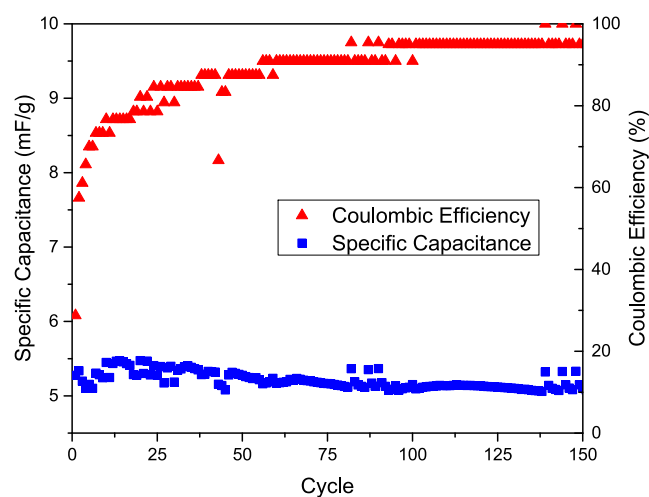
On the other hand, it can be elucidated that the values of the R-CPE element associated with the glass fiber separator are quite similar, as it depends on the nature of the separator, which is not significantly affected by the surface treatment of the carbon fiber electrodes. The adjustment by Nova 2.1 software is represented as solid lines in the graph of Fig. 9a.

Further electrochemical characterization by galvanostatic charge-discharge (GCD) was performed on the supercapacitor with electrodes made of GNP-coated carbon fiber without using any type of binder as it was the cell that showed higher specific capacitance in CV and the best R-CPE results from the EIS curves. A representative full cycle of GCD is shown in Fig. 10a.

A lack of linearity can be observed in both charge and discharge. This behavior can be associated with different causes such as parasitic reactions, high series resistance, or current leaks that generated uncompleted charge [58]. As stated before thanks to EIS analysis, there is a



(a)



(b)

**Fig. 10.** GCD behavior of the supercapacitors showing (a) a representative full cycle for each condition and (b) the specific capacitance and Coulombic efficiency under the first 150 cycles of the GNP-coated supercapacitor.

high internal resistance due to the solid polymer electrolyte even for the GNP-coated electrodes. The IR drop observed at the beginning of the discharge step is a consequence of the internal resistance. For this cell, the equivalent series resistance (ESR) is 24 k $\Omega$ . This initial IR drop is a highly limiting factor for the overall capacitive properties of the cells prepared with the GNP-PVA and GNP-PVDF electrodes, which ESR are 32.5 and 30 k $\Omega$  respectively.

The specific capacitance ( $C_{sp}$ ) for the GNP-coated fibers supercapacitor can be calculated from the discharge slope using Eq. (3) [49]. Where  $I$  (A) is the discharge current,  $\Delta t$  (s) is the discharge time,  $m$  (g) is the active mass of the electrode, and  $\Delta V$  (V) is the potential window for the charge-discharge process. At a current density of 0.02 mA/g, this cell can reach a capacity of 5.2 mF/g.

$$C_{sp} = \frac{I \cdot \Delta t}{m \cdot \Delta V} \quad (3)$$

The evolution of the supercapacitor behavior was tested on several

GCD cycles to evaluate the properties over time at the same current density. The coulombic efficiency (CE) can be calculated from the relation between the electrical charge storage during the charge ( $Q_c$ ) and the electrical charge release during discharge ( $Q_d$ ) as shown in Eq. (4) [49]. Where  $t_d$  and  $t_c$  are discharge and charge times, respectively, and  $I_d$  and  $I_c$  are the constant currents applied at discharge and charge, respectively.

$$CE (\%) = \frac{Q_d}{Q_c} \times 100 = \frac{I_d t_d}{I_c t_c} \times 100 \quad (4)$$

In Fig. 10b the values of specific capacitance and coulombic efficiency are shown. Over the first few cycles, the cell is stabilizing showing lower values of efficiency. After 150 cycles, the cell reaches a steady state with almost no loss of capacity from initial values and a coulombic efficiency close to 100 %. As supercapacitors are known to work on a longer number of cycles, it is relevant that a state of almost full efficiency is reached quickly without loss of capacitance. Therefore, these preliminary results proved that the proposed supercapacitor could work properly.

### 3.4. Proof-of-concept

As a proof-of-concept of the energy storage capabilities, a simple electrical arrangement was prepared with the goal of lighting an LED only powered with the developed structural supercapacitor. The device selected was the cell built with the GNP-coated fibers without binder as it offered the best electrochemical and mechanical capabilities. Before the proof-of-concept, the assembled supercapacitor was connected to a power supply at 10 V to charge it for 10 min. At this potential, the cell shows the capability to store and deliver energy although a deeper study is needed to evaluate the stability of the cell. After the charge, it was disconnected and connected to the LED. In this regard, Fig. 11a shows how the LED was lighted. After a few minutes, the LED intensity started to decrease as observed in Fig. 11b, c, and d. Also shown in the Supplementary Video File is the proof of concept and the connection between the LED and the cell.

Even after a short charge period, structural supercapacitors studied were able to prove their energy storage capabilities and show the potential of these devices. This proof-of-concept was previously carried out in other studies [59] but using a LED with a lower voltage (1.8 V against 3 V of the LED of the present study) and with a significantly bigger structural supercapacitor than the present study. Therefore, the proposed supercapacitor shows promising capabilities for energy storage.

## 4. Conclusions

The mechanical and electrochemical properties of a CFRP structural supercapacitor have been investigated.

In every case, the GNPs were deposited onto the carbon fiber surface, and the effect of the inclusion of a binder has been explored. It has been observed that the addition of a binder (PVA or PVDF) promotes a more prevalent GNP aggregation onto the carbon fiber surface.

Moreover, the inclusion of a binder promotes lower interfacial properties between the carbon fibers and the matrix, leading to a drastic reduction of the ILSS, especially when using a solid polymer electrolyte, due to a lack of impregnation caused by the more significant GNPs aggregation.

The electrochemical properties were evaluated through cyclic voltammetry and EIS analysis of the supercapacitors. The CV curves presented a similar EDCL pattern in every case, whereas the EIS curves were fitted accordingly to a series of R-CPE elements where the first one denotes the electrodes, the second one is the double layer, and the third one is the glass fiber separator. Here, the inclusion of a binder promotes a detriment on the electrochemical properties with both a reduction of the specific capacitance and an increase of the resistance associated with the electric double layer and the electrodes. In addition, an analysis of

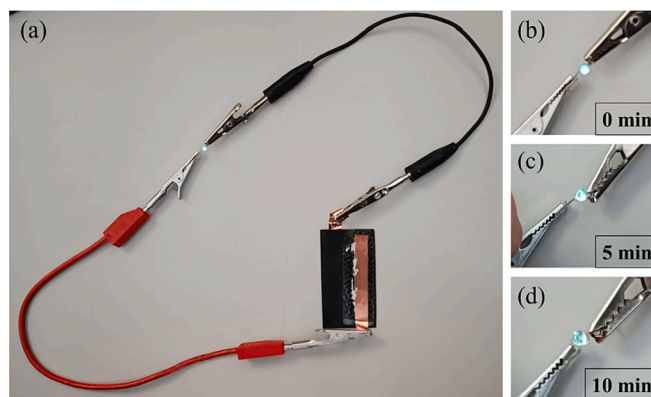


Fig. 11. Proof of concept of structural supercapacitor showing (a) test set-up and LED intensity at (b) the beginning of the test, (c) after 5 min, and (d) 10 min.

specific capacitance and coulombic efficiency of the GNP-coated supercapacitor was also conducted showing that, after 150 cycles, the cell reaches a steady state with almost no loss of capacity from initial values and a coulombic efficiency close to 100 % so it could work properly as a supercapacitor.

Finally, a proof-of-concept of the optimum structural supercapacitor, that is, the one coated only by GNPs was carried out by successfully powering a LED. Therefore, the proposed supercapacitor shows promising capabilities as an energy storage device. The use of other types of binders with much lower viscosities could help to improve the mechanical and electrochemical response.

Supplementary data to this article can be found online at <https://doi.org/10.1016/j.est.2022.106599>.

### CRediT authorship contribution statement

**Joaquín Artigas-Arnaudas:** Investigation, Methodology, Conceptualization, Formal analysis, Visualization, Writing – original draft. **Xoan F. Sánchez-Romate:** Methodology, Conceptualization, Formal analysis, Writing – original draft. **María Sánchez:** Writing – review & editing, Supervision, Funding acquisition. **Alejandro Ureña:** Supervision, Funding acquisition.

### Declaration of competing interest

The authors declare that they have no known competing financial interests or personal relationships that could have appeared to influence the work reported in this paper.

### Data availability

Data will be made available on request.

### Acknowledgements

This work was supported by the Agencia Estatal de Investigación of Spanish Government [Project MULTIFUNC-EVs PID2019-107874RB-I00] and Comunidad de Madrid Government [Project ADITIMAT-CM (S2018/NMT-4411)].

### References

- [1] M. Meinshausen, et al., Greenhouse-gas emission targets for limiting global warming to 2 °C, *Nature* 458 (7242) (2009) 1158–1162, <https://doi.org/10.1038/nature08017>.
- [2] G. Santos, Road transport and CO2 emissions: what are the challenges? *Transp. Policy* 59 (2017) 71–74, <https://doi.org/10.1016/j.tranpol.2017.06.007>.

- [3] S. Manzetti, F. Mariasiu, Electric vehicle battery technologies: from present state to future systems, *Renew. Sust. Energ. Rev.* 51 (2015) 1004–1012, <https://doi.org/10.1016/j.rser.2015.07.010>.
- [4] S. Ji, C.R. Cherry, M.J. Bechle, Y. Wu, J.D. Marshall, Electric vehicles in China: emissions and health impacts, *Environ. Sci. Technol.* 46 (4) (2012) 2018–2024, <https://doi.org/10.1021/es202347q>.
- [5] N.S. Pearre, W. Kempton, R.L. Guensler, V.V. Elango, Electric vehicles: how much range is required for a day's driving? *Transp. Res. Part C Emerg. Technol.* 19 (6) (2011) 1171–1184, <https://doi.org/10.1016/j.trc.2010.12.010>.
- [6] M.A. Hannan, M.M. Hoque, A. Mohamed, A. Ayob, Review of energy storage systems for electric vehicle applications: issues and challenges, *Renew. Sust. Energ. Rev.* 69 (2017) 771–789, <https://doi.org/10.1016/j.rser.2016.11.171>.
- [7] C. Reynolds, M. Kandlikar, How hybrid-electric vehicles are different from conventional vehicles: the effect of weight and power on fuel consumption, *Environ. Res. Lett.* 2 (1) (2007), 014003, <https://doi.org/10.1088/1748-9326/2/1/014003>.
- [8] B. Chatterjee, S. Bhowmik, Evolution of material selection in commercial aviation industry—a review, in: *Sustainable Engineering Products and Manufacturing Technologies*, Elsevier, 2019, pp. 199–219, <https://doi.org/10.1016/B978-0-12-816564-5.00009-8>.
- [9] S. Park, M. Seo, Carbon fiber-reinforced polymer composites: preparation, properties, and applications, in: S. Thomas, J. Kuruvilla, S.K. Malhotra, K. Goda, M. S. Sreekala (Eds.), *Polymer Composites*, 1st ed., Wiley, 2012, pp. 135–183, <https://doi.org/10.1002/9783527645213.ch5>.
- [10] L.E. Asp, E.S. Greenhalgh, Structural power composites, *Compos. Sci. Technol.* 101 (2014) 41–61, <https://doi.org/10.1016/j.compscitech.2014.06.020>.
- [11] C. González, J.J. Vilatela, J.M. Molina-Aldareguía, C.S. Lopes, J. Llorca, Structural composites for multifunctional applications: Current challenges and future trends, *Prog. Mater. Sci.* 89 (2017) 194–251, <https://doi.org/10.1016/j.pmatsci.2017.04.005>.
- [12] H. Zhou, et al., Structural composite energy storage devices — a review, *Mater. Today Energy* 24 (2022), 100924, <https://doi.org/10.1016/j.mtener.2021.100924>.
- [13] T. Christen, M.W. Carlen, Theory of ragone plots, *J. Power Sources* 91 (2) (2000) 210–216, [https://doi.org/10.1016/S0378-7753\(00\)00474-2](https://doi.org/10.1016/S0378-7753(00)00474-2).
- [14] B.E. Conway, *Electrochemical Supercapacitors: Scientific Fundamentals and Technological Applications*, Springer, US, Boston, MA, 1999, <https://doi.org/10.1007/978-1-4757-3058-6>.
- [15] X. Li, et al., Highly conductive, hierarchical porous ultra-fine carbon fibers derived from polyacrylonitrile/polymethylmethacrylate/needle coke as binder-free electrodes for high-performance supercapacitors, *J. Power Sources* 521 (2022), 230943, <https://doi.org/10.1016/j.jpowsour.2021.230943>.
- [16] P. Simon, Y. Gogotsi, Materials for electrochemical capacitors, *Nat. Mater.* 7 (11) (2008) 845–854, <https://doi.org/10.1038/nmat2297>.
- [17] Poonam, K. Sharma, A. Arora, S.K. Tripathi, Review of supercapacitors: materials and devices, *J. Energy Storage* 21 (2019) 801–825, <https://doi.org/10.1016/j.est.2019.01.010>.
- [18] S. Zheng, J. Zhang, H. Deng, Y. Du, X. Shi, Chitin derived nitrogen-doped porous carbons with ultrahigh specific surface area and tailored hierarchical porosity for high performance supercapacitors, *J. Bioresour. Bioprod.* 6 (2) (2021) 142–151, <https://doi.org/10.1016/j.jobab.2021.02.002>.
- [19] L. Wei, W. Deng, S. Li, Z. Wu, J. Cai, J. Luo, Sandwich-like chitosan porous carbon Spheres/MXene composite with high specific capacitance and rate performance for supercapacitors, *J. Bioresour. Bioprod.* 7 (1) (2022) 63–72, <https://doi.org/10.1016/j.jobab.2021.10.001>.
- [20] Q. Zhang, et al., Progress in the use of organic potassium salts for the synthesis of porous carbon nanomaterials: microstructure engineering for advanced supercapacitors, *Nanoscale* 14 (23) (2022) 8216–8244, <https://doi.org/10.1039/D2NR01986H>.
- [21] B. Yan, et al., Review on porous carbon materials engineered by ZnO templates: design, synthesis and capacitance performance, *Mater. Des.* 201 (2021), 109518, <https://doi.org/10.1016/j.matdes.2021.109518>.
- [22] B. Yan, et al., High performance supercapacitors based on wood-derived thick carbon electrodes synthesized via green activation process, *Inorg. Chem. Front.* 9 (23) (2022) 6108–6123, <https://doi.org/10.1039/D2QI01914K>.
- [23] X. Luo, D.D.L. Chung, Carbon-fiber/polymer-matrix composites as capacitors, *Compos. Sci. Technol.* 61 (6) (2001) 885–888, [https://doi.org/10.1016/S0266-3538\(00\)00166-4](https://doi.org/10.1016/S0266-3538(00)00166-4).
- [24] N. Shirshova, et al., Structural composite supercapacitors, *Compos. Part Appl. Sci. Manuf.* 46 (2013) 96–107, <https://doi.org/10.1016/j.compositesa.2012.10.007>.
- [25] H. Qian, et al., Activation of structural carbon fibers for potential applications in multifunctional structural supercapacitors, *J. Colloid Interface Sci.* 395 (2013) 241–248, <https://doi.org/10.1016/j.jcis.2012.12.015>.
- [26] H. Qian, A.R. Kucernak, E.S. Greenhalgh, A. Bismarck, M.S.P. Shaffer, Multifunctional structural supercapacitor composites based on carbon aerogel modified high performance carbon fiber fabric, *ACS Appl. Mater. Interfaces* 5 (13) (2013) 6113–6122, <https://doi.org/10.1021/am400947j>.
- [27] A. Javid, M. Irfan, Multifunctional structural supercapacitors based on graphene nanoplatelets/carbon aerogel composite coated carbon fiber electrodes, *Mater. Res. Express* 6 (1) (2018), 016310, <https://doi.org/10.1088/2053-1591/aae862>.
- [28] N. Shirshova, et al., Multifunctional structural energy storage composite supercapacitors, *Faraday Discuss.* 172 (2014) 81–103, <https://doi.org/10.1039/C4FD00055B>.
- [29] J. Karger-Kocsis, H. Mahmood, A. Pegoretti, All-carbon multi-scale and hierarchical fibers and related structural composites: a review, *Compos. Sci. Technol.* 186 (2020), 107932, <https://doi.org/10.1016/j.compscitech.2019.107932>.
- [30] B.K. Deka, A. Hazarika, J. Kim, Y.-B. Park, H.W. Park, Multifunctional CuO nanowire embodied structural supercapacitor based on woven carbon fiber/ionic liquid–polyester resin, *Compos. Part Appl. Sci. Manuf.* 87 (2016) 256–262, <https://doi.org/10.1016/j.compositesa.2016.05.007>.
- [31] B.K. Deka, A. Hazarika, O.B. Kwon, D. Kim, Y.-B. Park, H.W. Park, Multifunctional enhancement of woven carbon fiber/ZnO nanotube-based structural supercapacitor and polyester resin-domain solid-polymer electrolytes, *Chem. Eng. J.* 325 (2017) 672–680, <https://doi.org/10.1016/j.cej.2017.05.093>.
- [32] J. Sun, et al., Recent progress of fiber-shaped asymmetric supercapacitors, *Mater. Today Energy* 5 (2017) 1–14, <https://doi.org/10.1016/j.mtener.2017.04.007>.
- [33] Q. Zhang, J. Liu, R. Sager, L. Dai, J. Baur, Hierarchical composites of carbon nanotubes on carbon fiber: influence of growth condition on fiber tensile properties, *Compos. Sci. Technol.* 69 (5) (2009) 594–601, <https://doi.org/10.1016/j.compscitech.2008.12.002>.
- [34] J. Artigas-Arnaudas, B.K. Muñoz, M. Sánchez, J. de Prado, M.V. Utrilla, A. Ureña, Surface modifications of carbon fiber electrodes for structural supercapacitors, *Appl. Compos. Mater.* (2021), <https://doi.org/10.1007/s10443-021-09998-5>.
- [35] O. Hubert, N. Todorovic, A. Bismarck, Towards separator-free structural composite supercapacitors, *Compos. Sci. Technol.* 217 (2022), 109126, <https://doi.org/10.1016/j.compscitech.2021.109126>.
- [36] A.M. A. Paul, Importance of electrode preparation methodologies in supercapacitor applications, *ACS Omega* 2 (11) (2017) 8039–8050, <https://doi.org/10.1021/acsomega.7b01275>.
- [37] S. Rajeevan, S. John, S.C. George, Polyvinylidene fluoride: a multifunctional polymer in supercapacitor applications, *J. Power Sources* 504 (2021), 230037, <https://doi.org/10.1016/j.jpowsour.2021.230037>.
- [38] S. Alipoori, S. Mazinani, S.H. Aboutalebi, F. Sharif, Review of PVA-based gel polymer electrolytes in flexible solid-state supercapacitors: opportunities and challenges, *J. Energy Storage* 27 (2020), 101072, <https://doi.org/10.1016/j.est.2019.101072>.
- [39] A. Masouras, D. Giannopoulos, B. Hasa, A. Katsaounis, V. Kostopoulos, Hybrid graphene nanoplatelet/manganese oxide electrodes for solid-state supercapacitors and application to carbon fiber composite multifunctional materials, *J. Energy Storage* 23 (2019) 515–525, <https://doi.org/10.1016/j.est.2019.04.025>.
- [40] J. Sun, et al., Mechanical and electrochemical performance of hybrid laminated structural composites with carbon fiber/ solid electrolyte supercapacitor interleaves, *Compos. Sci. Technol.* 196 (2020), 108234, <https://doi.org/10.1016/j.compscitech.2020.108234>.
- [41] K. Friedrich, U. Breuer, *Multifunctionality of Polymer Composites*, Elsevier, 2015, <https://doi.org/10.1016/C2013-0-13006-1>.
- [42] B.K. Muñoz, et al., Epoxy resin systems modified with ionic liquids and ceramic nanoparticles as structural composites for multifunctional applications, *Polymer* 214 (2021), 123233, <https://doi.org/10.1016/j.polymer.2020.123233>.
- [43] A. Javid, K. Ho, A. Bismarck, M. Shaffer, J. Steinke, E. Greenhalgh, Multifunctional structural supercapacitors for electrical energy storage applications, *J. Compos. Mater.* 48 (12) (2014) 1409–1416, <https://doi.org/10.1177/0021998313487239>.
- [44] S. Cheng, D.M. Smith, C.Y. Li, How does nanoscale crystalline structure affect ion transport in solid polymer electrolytes? *Macromolecules* 47 (12) (2014) 3978–3986, <https://doi.org/10.1021/ma500734q>.
- [45] A. del Bosque, B.K. Muñoz, M. Sánchez, A. Ureña, Thermomechanically robust Ceramic/Polymer nanocomposites modified with ionic liquid for hybrid polymer electrolyte applications, *ACS Appl. Energy Mater.* 5 (4) (2022) 4247–4258, <https://doi.org/10.1021/acsaem.1c03836>.
- [46] A. Javid, O. Khalid, A. Shakeel, S. Noreen, Multifunctional structural supercapacitors based on polyaniline deposited carbon fiber reinforced epoxy composites, *J. Energy Storage* 33 (2021), 102168, <https://doi.org/10.1016/j.est.2020.102168>.
- [47] D.D.L. Chung, Development, design and applications of structural capacitors, *Appl. Energy* 231 (2018) 89–101, <https://doi.org/10.1016/j.apenergy.2018.09.132>.
- [48] X.F. Sánchez-Romate, A.D. Bosque, J. Artigas-Arnaudas, B.K. Muñoz, M. Sánchez, A. Ureña, A proof of concept of a structural supercapacitor made of graphene coated woven carbon fibers: EIS study and mechanical performance, *Electrochim. Acta* 370 (2021), 137746, <https://doi.org/10.1016/j.electacta.2021.137746>.
- [49] S. Zhang, N. Pan, Supercapacitors performance evaluation, *Adv. Energy Mater.* 5 (6) (2015) 1401401, <https://doi.org/10.1002/aenm.201401401>.
- [50] B. Yan, et al., Nitrogen-doped carbon layer on cellulose derived free-standing carbon paper for high-rate supercapacitors, *Appl. Surf. Sci.* 608 (2023), 155144, <https://doi.org/10.1016/j.apsusc.2022.155144>.
- [51] J. Zheng, et al., Potassium citrate assisted synthesis of hierarchical porous carbon materials for high performance supercapacitors, *Diam. Relat. Mater.* 128 (2022), 109247, <https://doi.org/10.1016/j.diamond.2022.109247>.
- [52] L. Feng, et al., Soybean protein-derived N, O co-doped porous carbon sheets for supercapacitor applications, *New J. Chem.* 46 (22) (2022) 10844–10853, <https://doi.org/10.1039/D2NJ01355J>.
- [53] N.A. Cañas, K. Hirose, B. Pascucci, N. Wagner, K.A. Friedrich, R. Hiesgen, Investigations of lithium–sulfur batteries using electrochemical impedance spectroscopy, *Electrochim. Acta* 97 (2013) 42–51, <https://doi.org/10.1016/j.electacta.2013.02.101>.
- [54] M. Frankenberger, M. Singh, A. Dinter, K.-H. Pettinger, EIS study on the electrode-separator Interface lamination, *Batteries* 5 (4) (2019) 71, <https://doi.org/10.3390/batteries5040071>.
- [55] R.T. Abdulwahid, S.B. Aziz, M.F.Z. Kadir, Insights into ion transport in biodegradable solid polymer blend electrolyte based on FTIR analysis and circuit

- design, *J. Phys. Chem. Solids* 167 (2022), 110774, <https://doi.org/10.1016/j.jpcs.2022.110774>.
- [56] R.T. Abdulwahid, S.B. Aziz, M.F.Z. Kadir, Design of proton conducting solid biopolymer blend electrolytes based on chitosan-potato starch biopolymers: deep approaches to structural and ion relaxation dynamics of H<sup>+</sup> ion, *J. Appl. Polym. Sci.* 139 (37) (2022), <https://doi.org/10.1002/app.52892>.
- [57] S. Kochowski, K. Nitsch, Description of the frequency behaviour of metal-SiO<sub>2</sub>-GaAs structure characteristics by electrical equivalent circuit with constant phase element, *Thin Solid Films* 415 (1–2) (2002) 133–137, [https://doi.org/10.1016/S0040-6090\(02\)00506-0](https://doi.org/10.1016/S0040-6090(02)00506-0).
- [58] T.S. Mathis, N. Kurra, X. Wang, D. Pinto, P. Simon, Y. Gogotsi, Energy storage data reporting in Perspective—Guidelines for interpreting the performance of electrochemical energy storage systems, *Adv. Energy Mater.* 9 (39) (2019) 1902007, <https://doi.org/10.1002/aenm.201902007>.
- [59] B.K. Deka, et al., Bimetallic copper cobalt selenide nanowire-anchored woven carbon fiber-based structural supercapacitors, *Chem. Eng. J.* 355 (2019) 551–559, <https://doi.org/10.1016/j.cej.2018.08.172>.